Combining X-ray Absorption and X-ray Diffraction Techniques for in Situ Studies of Chemical Transformations in Heterogeneous Catalysis: Advantages and Limitations

A. I. Frenkel,*,[†] Q. Wang,[‡] N. Marinkovic,[‡] J. G. Chen,[‡] L. Barrio,[§,‖] R. Si,[§] A. López Cámara,[‖] A. M. Estrella,[§] J. A. Rodriguez,[§] and J. C. Hanson*,[§]

[†]Department of Physics, Yeshiva University, New York, New York 10016, United States

[‡]Department of Chemical Engineering, University of Delaware, Newark, Delaware 19716, United States

[§]Department of Chemistry, Brookhaven National Laboratory, Upton, New York 11973, United States

[‖]Instituto de Catálisis y Petroleoquímica, CSIC, Marie Curie 2, 28049 Madrid, Spain

Ⓢ *Supporting Information*

ABSTRACT: Recent advances in catalysis instrumentations include synchrotron-based facilities where time-resolved X-ray scattering and absorption techniques are combined in the same in situ or operando experiment to study catalysts at work. To evaluate the advances and limitations of this method, we performed a series of experiments at the new XAFS/XRD instrument in the National Synchrotron Light Source. Nearly simultaneous X-ray diffraction (XRD) and X-ray absorption fine-structure (XAFS) measurements of structure and kinetics of several catalysts under reducing or oxidizing conditions have been performed and carefully analyzed. For $CuFe_2O_4$ under reducing conditions, the combined use of the two techniques allowed us to obtain accurate data on kinetics of nucleation and growth of metallic Cu. For the inverse catalyst CuO/CeO_2 that underwent isothermal reduction (with CO) and oxidation (with O_2), the XAFS data measured in the same experiment with XRD revealed strongly disordered Cu species that went undetected by diffraction. These and other examples emphasize the unique sensitivity of these two complementary methods to follow catalytic processes in the broad ranges of length and time scales.
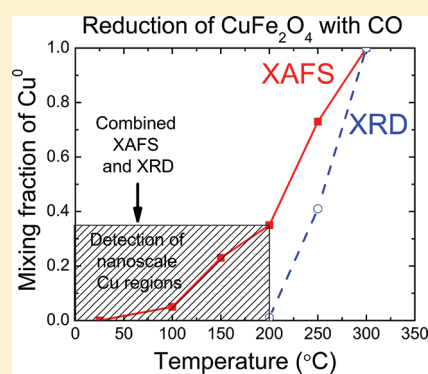
I. INTRODUCTION

Investigation of the structure, dynamics, and electronic properties of catalysts in real time and under reaction conditions is essential for elucidating reaction pathways and kinetics. Among other techniques, synchrotron X-ray absorption fine-structure (XAFS) spectroscopy and diffraction (XRD) are the ones most commonly used for in situ and operando research. Using time-resolved XRD, one can get information concerning the following properties: phase identification, fractional composition, crystalline properties, and molecular structure of catalysts under reaction conditions, as well as kinetics of crystallization of nanoparticles and bulk solids.

Time-resolved XAFS allows one to follow the structural changes in the reactions with characteristic times ranging from minutes to tens of milliseconds. Most applications of time-resolved XAS use either energy dispersive[1−5] or energy scanning mode.[6−9]

For more than 10 years researchers have been conducting subminute, time-resolved in situ XRD experiments under a wide variety of temperature and pressure conditions (80 K < T < 1200 K; P < 50 atm).[10] These advances result from combining the high intensity of synchrotron radiation with new parallel data-collection devices. A recent in situ study of the active phase of CuO−CeO$_2$ catalysts during the water gas shift (WGS) reaction[11] illustrates both the power, and the limitations, of time-resolved XRD and time-resolved XAFS at separate beamlines available for the characterization of catalysts at the National Synchrotron Light Source (NSLS). In that work, the partial reduction of cerium in the ceria was determined from very different measurements. Ce L$_3$ edge XANES spectra measured at X18B beamline as a function of temperature under WGS conditions showed the variation of the relative amounts of Ce^{3+} and Ce^{4+} cations. The XRD data, obtained at the X7B beamline, also indicated, albeit in a less direct way, that the amount of Ce^{3+} in the catalyst varies with the CO/H_2O ratio. That result was inferred from the change in the cerium oxide lattice parameter at constant temperature. The lattice is sensitive to the presence of Ce^{3+} and expands (or contracts) when the concentration of this cation increases (or decreases), in accordance with the Vegard's law.

That work (ref 11) demonstrates that the both sets of data provide information about vacancies in the catalysts, but there are important details about the system that are missing in each of them. XAFS is sensitive to the local structure only, within a few coordination shells around the absorbing atom. In systems with small to moderate disorder, XAFS can characterize local structure accurately even if the long-range order is absent. However, because of its local nature, XAFS is not capable of characterizing the volume of each structurally/compositionally different region in the sample, nor can it tell whether these regions are ordered or disordered. On the other hand, Bragg diffraction originates from coherent scattering and thus requires long-range periodicity within a region at least a few unit cells in size. Thus, it will detect ordered phases only but will underestimate the contribution of strongly disordered and/or low dimensional phases, as well as metastable reaction intermediates. Such contributions are a very common phenomenon in catalytic processes.

A recent example is the work by Piovano et al.,[12] studying electrochemical oxygen intercalation in $SrFeO_{2.5}$ by separately using Fe K-edge extended XAFS (EXAFS) and neutron diffraction in the same system. No disordered contribution was observed in the diffraction experiment in this system during its electrochemical oxidation. However, principal component analysis of XANES and EXAFS data has shown the presence of an intermediate phase. By comparing the results of these two experiments, the authors of ref 12 concluded that the unknown phase is strongly disordered, which explains why it was observed by XAFS and not XRD.[13] To avoid such factors as irreproducibility of reaction conditions (due to, e.g., thermal/compositional gradients in the reactor and/or radiation-induced changes of the electronic state or structure of the sample) and to obtain internally consistent structural and kinetic information about catalytic reaction, one needs to combine fast XAFS and fast XRD in a single experiment under in situ conditions, coupled with online product analysis.[14]

The pioneering work of Thomas[15] and Clausen[8] on combining XRD and XAFS in one single experiment with enough time resolution to follow the kinetics of structural changes of solids under in situ conditions opened the door to the employment of a powerful characterization tool for unraveling complex structural transformations and its application to mixed oxides systems. Further developments in the technique increased the resolution of both the XRD and XAFS measurements.[16] In this article we introduce an experimental setup (section II) for such investigations built at beamline X18A of the NSLS and demonstrate its applicability for in situ studies of catalytic reactions. Examples shown below will emphasize complementary qualities of each technique by pointing out what information revealed by one technique is not accessible by the other. This complementarity will be exploited to advance our understanding of the *actual* structure, which combines local and average information of the catalytic systems.

II. COMBINED XAFS/XRD INSTRUMENT

The setup for combined QEXAFS/XRD investigations was built in the endstation of the X18A bending magnet beamline. The beamline has a channel cut Si (111) monochromator with an energy range of ∼5−40 keV. Focusing is achieved by a Rh-coated, toroidal mirror. The monochromator uses an eccentric cam that can be driven by a dc motor and a tangent arm at a 0.1−1.2 Hz frequency. Alternatively, the five-phase stepping motor can be used for scanning at standard speeds for regular

XAFS.[17] Quick EXAFS (QEXAFS) data can be collected in 0.5 s (for concentrated samples), and in 5−15 s for dilute (∼1 wt % catalyst loading) ones.

Three X-ray detectors were used in the XRD measurements described in this work. They include an INEL linear curved detector mounted on the 2θ arm, a silicon linear detector (SiLD), and a Perkin Elmer (PE) amorphous silicon detector. SiLD is a microstrip array of silicon diodes (800 elements, 0.125 × 4 mm^2 in area per element), designed and made at BNL.[18] It is mounted on the 2θ arm and can be used in stationary mode. It has ca. 10° acceptance angle, the readout time (low limit) is 0.03 s, and the typical exposure time in the experiments described below is 30 s. A PE detector is the one most commonly used. It has 2048 × 2048 pixels and a 200 × 200 μm^2 pixel size. The detector records patterns with an area of 40 × 40 cm^2. The detector is mounted on the 2θ arm, the typical 2θ range is 5 to 48°, and the typical exposure in the experiments described below was 30 s.

The XAFS data were usually collected in the fluorescence mode with a passivated implanted planar silicon (PIPS) detector. For concentrated samples, where fluorescence signal suffers from thickness effect, a steady state measurement is taken as well, in fluorescence and transmission modes. Such measurement is then used to recover the constant amplitude factor that, to a good approximation, corrects for the thickness effect.[19]

The reaction products of the in situ experiments described below are measured with a 0−100 amu quadruple mass spectrometer (QMS, Stanford Research Systems). More details about this setup and additional detectors available at X18A beamline for combined QEXAFS/XRD can be found in ref 17.

III. STRUCTURAL TRANSFORMATIONS OF CUFE$_2$O$_4$ UNDER CO FLOW AT ELEVATED TEMPERATURES

Cuprospinel $CuFe_2O_4$ is a well-known precursor for copper catalysts with high thermal stability and activity. It is used as a catalyst in hydrogen production and thermal decomposition of ammonium perchlorate and is potentially useful for the WGS reaction.[20] The copper spinel has an inverse structure in which the Cu^{2+} cations occupy the octahedral positions of the tetragonal unit cell whereas Fe^{2+} and Fe^{3+} cations split between octahedral and tetrahedral positions of the crystalline cell. The reduction of this copper spinel with hydrogen and carbon monoxide has been previously studied by separate XRD and XAFS measurements.[20] Copper cations segregate out of the structure under reducing conditions at high enough temperatures and, again under oxidizing conditions, copper readily reincorporates back into the spinel structure. Its structural transformation upon reduction cannot be fully understood by the XRD technique alone, due to the likelihood of forming metastable, short living, strongly dispersed, and/or disordered phases toward the formation of pure Cu, similar to the observation done in ref 12. Only by combining XRD and XAFS in a single experiment, where the sample is subjected to the same temperature/gas treatment conditions, can one detect both the short-range and the long-range structure of this system and ensure that the two results describe the same chemical and physical states of the sample.

The following two sections present two different studies (performed with INEL and SiLD XRD detectors) of $CuFe_2O_4$ during the reduction with CO. The INEL has been traditionally used in XRD/XAS measurements and measures the whole
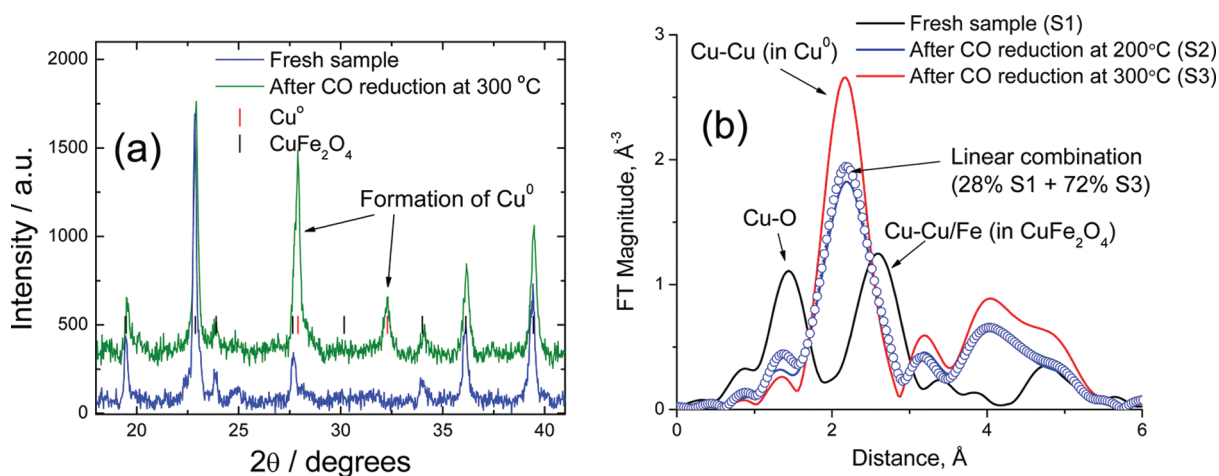
Figure 1. Results of combined XAFS/XRD measurements of temperature-dependent reduction of $CuFe_2O_4$ in CO.

pattern but saturates at our X-ray flux. The SiLD is a new detector that provides much more rapid readout, but with limited angular range. For experiments where the X-ray determination is based on the peak height of the metallic copper phase, the limited range is acceptable.

The sample was loaded in a $^1/_8$ in. Kapton tube in a flow cell. The XAFS was measured with a PIPS detector (the sample was too thick to allow for measurement of transmission or reference signal). The temperature was controlled with an air blower that was placed below the sample.

The first study was performed using the INEL linear detector. The XRD data were collected at 25, 200, 250, and 300 °C and after cooling to 25 °C. The data were collected at a wavelength of 1 Å and with a full readout time of 5 min. The time required to move the monochromator from 12 398 eV (corresponding to the wavelength of 1 Å) to the Cu K-edge (8979 eV) was ca. 1 min. The EXAFS data were analyzed after averaging over three consecutive EXAFS scans. Figure 1a shows XRD data of the fresh sample and that reduced under CO flow at 300 °C and then cooled to room temperature. The latter sample, according to XRD, is a mixture of two phases: the reduced Cu and the Fe_3O_4. Figure 1b shows Fourier transform magnitudes of EXAFS data, demonstrating that the sample reduced at 200 °C and cooled to room temperature is a linear combination of the fresh sample and the fully reduced sample that was heated to 300 °C under CO and then cooled to room temperature. Linear combination analysis was performed on the data in k-space. Fourier transforms are shown to better illustrate different copper environments in the sample.

From the XRD data one can obtain an estimate of the amount of metallic copper phase from the ratio of the peak height of the (200) reflection at a given temperature to the peak height of the fully reduced sample at 300 °C. The diffraction peak height data indicate that the metallic phase fraction is somewhat lower at 200 °C than that shown in Figure 1b. This difference can be interpreted as the presence of a small fraction of disordered/amorphous Cu that is difficult to detect by XRD but noticeable to XAFS.

Because the two measurements were done on the same sample going through the same chemical treatment, their results are internally consistent and offer an unambiguous interpretation (vide supra). This interpretation is also independently confirmed by a separate measurement with a SiLD detector (vide infra).

In the second study of the $CuFe_2O_4$ XRD data were measured with the SiLD detector. The measurements were collected in an identical setup as described above. The sample was "activated" by heating at 200 °C in a 10% O_2/He flow. The sample was then reduced at different temperatures while XRD and XAFS measurements were taken (the XAFS measurements were made between sequential XRD measurements) on the same sample under identical conditions. The XRD measurements were made 50 eV below the Cu K-edge to minimize the monochromator movement time between the XAFS and XRD measurements. Here we present the Cu and Fe K-edge spectra and the diffraction measurements followed by a comparison of the results.

Figure 2a shows XANES data of Cu K edge in CO flow at various temperatures. It shows that with increasing temperature, the white line shifts to lower energy and decreases in intensity, indicating that the reaction gradually changes copper to lower oxidation states than the initial Cu(II). A characteristic shoulder indicating the formation of metallic Cu emerges in the Cu edge data at 150 °C. The XANES features at 300 °C are already close to those of a pure metallic Cu. During the entire temperature series the data feature several isosbestic points, indicating a one-step transformation.

The Fe K-edge XANES data (Figure 2b) reveal a gradual shift to lower energies, and a reduction in the peak intensity with temperature, consistent with the gradual reduction of Fe as temperature increases. In contrast to Cu behavior, Fe remains oxidized throughout the entire temperature range used. Because Cu occupies octahedral positions only, it is expected that the proportion of Fe in octahedral sites vacated by Cu increases with temperature. Because Fe^{3+} ions can occupy both tetrahedral and octahedral sites, whereas Fe^{2+} can be found only in the octahedral sites,[21] we expect that the factor limiting the rate of Fe reduction is the rate of formation of vacancies on octahedral sites, i.e., the rate of Cu reduction. The combination of the Cu and Fe K-edge XANES data behaviors measured in the same in situ experiment suggests that Fe occupies vacancies generated in the spinel structure by the reduction of copper. Hence, it is expected that the rates of the Cu and Fe reductions must be similar, which is indeed confirmed by the quantitative data analysis of Cu and Fe XANES (vide infra).

Figure 3 shows the XRD data in the region where Cu peaks appear during reduction of the cuprospinel. There are slight
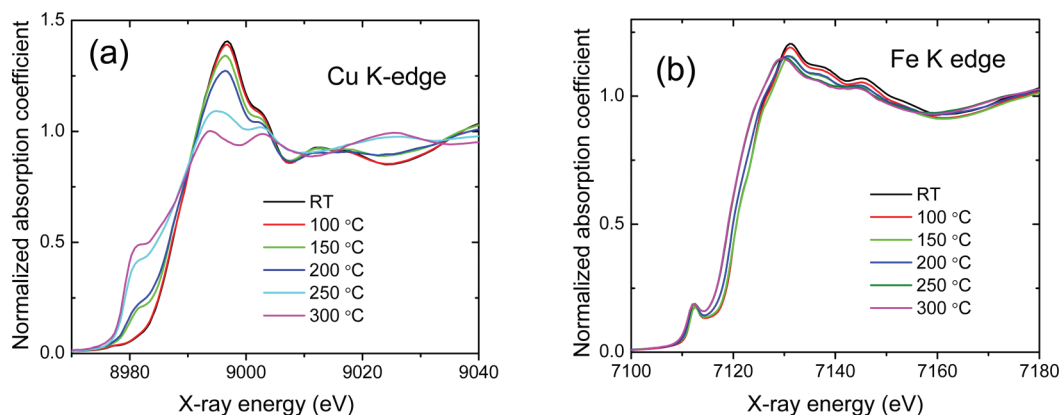
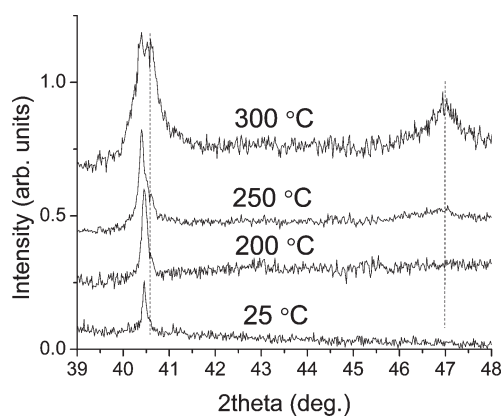**Figure 2.** XANES data of Cu K-edge (a) and Fe K-edge (b) of $CuFe_2O_4$ in CO flow at various temperatures.

Figure 3. XRD data at different temperatures under CO reducing conditions. The Cu^0 phase appears near $40.5°$ and $47°$. The peak near $40.5°$ overlaps with a spinel peak, but the peak near $47°$ is only from (200) Cu^0. The normalized integrated areas of this peak at different temperatures are presented in Table 1.

Figure 4. Comparison of Cu^0 and $Fe^{\delta+}$ fractions determined by XRD and XAS at different temperatures.

changes in the diffraction pattern when the Cu^{2+} cations leave the oxide and the pure magnetite phase is formed. First, there is a change in the relative peak intensities due to the change in the occupancy of the octahedral sites. There is also a small shift on the peak position due to a cell dimension change when copper segregates from the oxide. This shift can, therefore, be related to the relative amounts of cuprospinel and magnetite. The amount of the metallic copper phase can be estimated from the (200) peak height ratio as discussed in the previous section.

Quantitative analyses of the XRD and XAFS measurements were done as follows. The volume mixing fractions of reduced and unreduced Cu and Fe were obtained from the Cu K-edge and Fe K-edge XANES data analysis, respectively (Figure 4 and Table 1). To obtain these quantities, we performed linear combination fits of the room temperature (most oxidized) data and 300 °C (most reduced) data to the XANES signals measured at all the intermediate temperatures. Typical accuracy of the mixing fraction measurement by this method was ±0.05 or better. The amounts of phase fraction of the Cu^0 species using XRD data were determined from the integrated peak intensity of the Cu 200 reflection.[22] The relative amounts of metallic copper phase obtained by XRD are also given in Table 1.
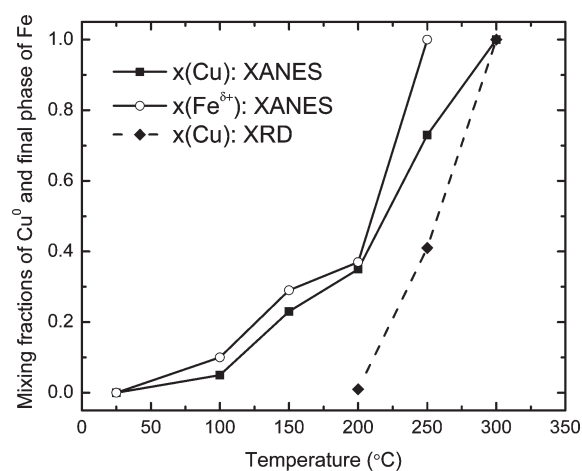
EXAFS analysis provided unique information about the rates of reduction of Fe and Cu in the complex system. The fact that the temperature dependences of transforming both of these species are in good agreement with each other points to a specific mechanism in which Fe occupies octahedral sites vacated by Cu, as suggested above.

It should also be pointed out that both EXAFS and XRD analyses results give no hint of the presence of any copper species other than the initial spinel and the final metallic Cu^0. The comparison between the EXAFS and XRD results offers a conclusion, same as that indicated from the independent experiment with INEL detector (vide supra) that there is an underestimation of relative amount of Cu^0 by XRD at the intermediate temperature range. This is consistent with Cu^0 appearing as an amorphous, and/or low-dimensional, phase prior to the appearance of the crystalline phase.

IV. IN SITU STUDIES OF STRUCTURAL TRANSFORMATIONS OF THE CU/CERIA INVERSE CATALYST

The previous examples demonstrate that important conclusions about the phase composition of a mixed system can be made by cointerpreting the results of two measurements on a sample that partially reduced during in situ chemical transformations. In that

Table 1. Temperature-Dependent Volume Mixing Fractions of the Final States of Cu (Metal) and Fe (Consistent with Magnetite) during the in Situ XAFS Experiments[a]

T (°C)	x(Cu) XAFS	x(Fe$^{\delta+}$) XAFS	x(Cu) XRD
25	0	0	0
100	0.05	0.1	
150	0.23	0.29	
200	0.35	0.37	0.01
250	0.73	1	0.41
300	1	1	1

[a] The XRD-derived fraction of reduced metal Cu is given for comparison.

Figure 5. XRD data of the inverse Cu/ceria catalyst before and after reduction.

case, we ruled out a reaction intermediate and concluded in favor of a one-step process. The following example demonstrates how the XRD and XAFS measurements, at the first glance, appear to contradict each other in the results they report. In this experiment, we investigated structural transformations in the CuO/Cu$_x$Ce$_{1-x}$O$_2$ ("inverse Cu/ceria") catalyst during CO reduction and subsequent reoxidation with O$_2$. The as prepared sample is a mixture of a CuO phase and a Cu$_x$Ce$_{1-x}$O$_2$ with a Cu/Ce ratio of 6/4 as determined by X-ray fluorescence.[23,24] The inverse nature of the catalyst is illustrated from the diffraction patterns that show broad peaks due to the nanosize of CeO$_2$ crystals and well-defined peaks for the CuO phase. It has been also independently confirmed by HR-TEM.[24] Upon reduction, the signal of Cu^0 produced very sharp peaks, indicating the bulk nature of the metallic phase (Figure 5).

This system is a new WGS catalyst that is attractive in mobile applications due to its high activity at low temperatures and stability during redox cycles.[23] This inverse system has also proven to be a highly efficient catalyst for the preferential CO oxidation reaction, because the presence of bulk-like copper structures quenches the hydrogen oxidation reaction, therefore providing a wider range of operating temperatures than a conventional Cu/CeO$_2$ system.[24]

Previous studies of the system by separate XAFS and XRD experiments showed a strong interaction between copper and ceria crystallographic phases due to the high mobility of oxygen interchange between them, but the existing data were inconclusive as to the presence, and the nature, of intermediate transitions. The combined XRD/XAFS measurements can quantify the composition of Cu in the two phases and characterize their structures (including the local structure in the disordered and/or low-dimensional phases) and oxidation states.

The sample cell was the same as in the CuFe$_2$O$_4$ experiment described above. XRD patterns (measured with 30 s exposure time) were collected at 20 keV during reduction by flowing 5% CO/He mixture at the flow rate of 10 cc/min while increasing the temperature from RT to 200 °C and during oxidation experiments, where the 20% O$_2$/He mixture was introduced at 200 °C with 10 cc/min flow rate, and the temperature was held at 200 °C, then increased and held at 250 and 300 °C. XAFS scans were collected before and after the CO reduction at 25 and 200 °C. XAFS scans were also collected during the reoxidation experiment (at the end of the 30 min exposure to O$_2$) and at 300 °C (after the extended exposure to O$_2$). Gases leaving the reaction chamber were analyzed with a quadruple mass spectrometer (QMS). The Supporting Information, section S1, shows the details of this product evolution.
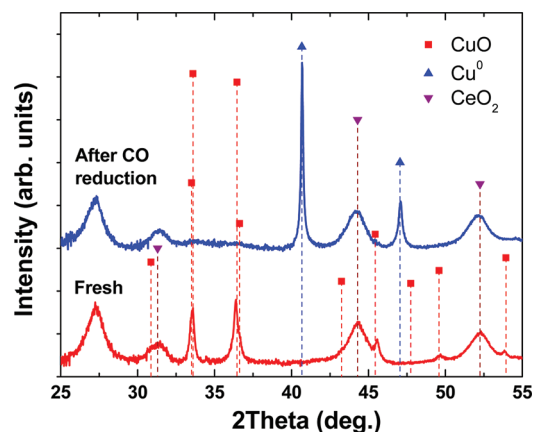
Two-dimensional powder XRD patterns were integrated using the FIT2D code.[25] Lattice parameters and phase fractions were determined through Rietveld refinement[26] by using the GSAS software.[27] The results of the time-resolved XRD measurements are shown in Figure 6 and Table 2. From Figure 6a, it can be seen that CuO in the fresh inverse catalyst was directly reduced to Cu metal in 5% CO/He below 200 °C. No intermediate phase (Cu$_2$O) was observed. In Figure 6b, the reoxidation resulted in the mixture of CuO and Cu$_2$O at 200 °C in 20% O$_2$/He, and Cu$_2$O was found to be fully oxidized at 300 °C. The above results demonstrate that the Cu$_2$O intermediate structure is only stable in the reoxidation step.

Cu K-edge XAFS measurements were performed by a scanning data collection mode. XANES data in Figure 7 (inset) show the transformations of the fresh sample upon CO reduction and subsequent reoxidation. The fresh sample was found to be dominated by Cu^{2+}, and the reoxidized sample at 300 °C was found to be identical with the fresh sample, in the XANES region (Figure 7). Linear combination fits of XANES data provided the mixing fractions of Cu^0, Cu$^+$, and Cu^{2+} in the reduced and reoxidized samples. For the linear combination analysis the XANES data measured in Cu metal foil, CuO and Cu$_2$O powder data were used as standards for the Cu^0, Cu$^+$, and Cu^{2+} oxidation states, respectively. In addition, a standard for the substitutional phase Cu:CeO$_2$ was also used.[28] To account for the temperature difference between the Cu/ceria data and the standards (collected at room temperature), a minor smoothening was applied to the XANES data of the Cu and CuO standards before the linear combination fit was done.

Numerical results for the XANES and XRD data analyses are summarized in Table 2. Both techniques revealed that the chemical state of Cu in the starting sample, as well as in the sample reoxidized at 300 °C, was Cu^{2+}. In the sample that was reduced and then subsequently oxidized at 200 °C, the two techniques reported different amounts of Cu^0, Cu$^+$, and Cu^{2+}. In the both cases, XRD underestimated the amounts of *minority* phases in the sample (Cu$^+$ and Cu^{2+} in the reduced sample and Cu^0 and Cu$^+$ in the oxidized sample). One can conclude that the reduced sensitivity of XRD to these contributions was likely to be caused by the enhanced disorder and/or low dimensionality of these undetected phases. XAFS, being a local structural method, is sensitive to the local structure only, and is thus more likely to detect such phases (Table 1). However, without the simultaneous
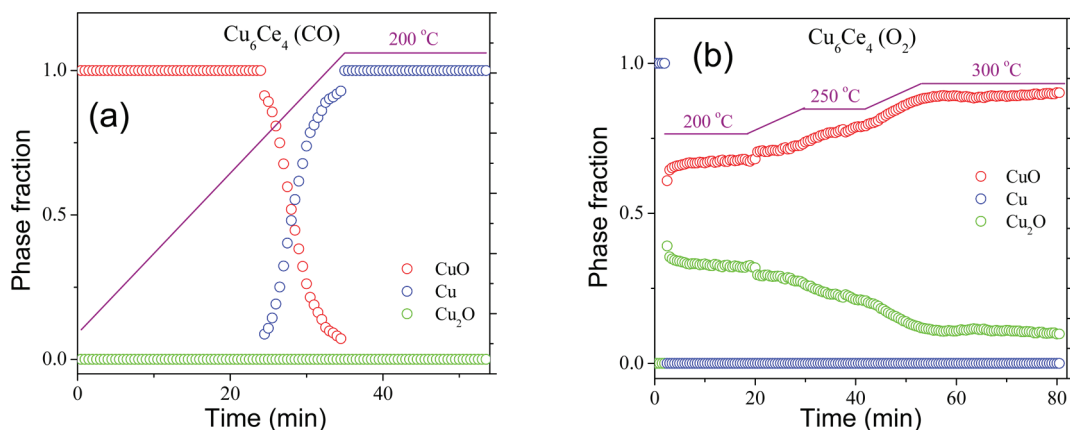
17888

dx.doi.org/10.1021/jp205204e |*J. Phys. Chem. C* 2011, 115, 17884–17890

Figure 6. Molar phase fraction of copper species during reduction (a) and reoxidation (b), as measured by the XRD.

Table 2. Mixing Fractions of Cu^0, Cu$^+$, and Cu^{2+} in the Inverse Cu/Ceria Catalysts Obtained during CO Reduction and O$_2$ Oxidation by XAFS and XRD Techniques in a Single Experiment

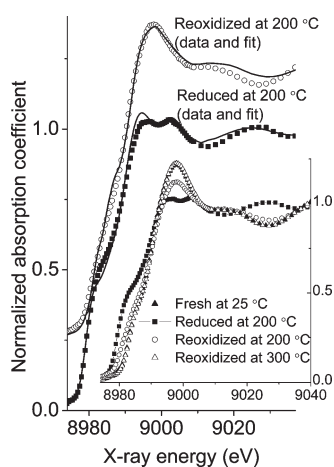| | Cu^0 | | Cu$^+$ | | Cu^{2+} in CuO | | Cu^{2+} in CeO$_2$ | |
sample	XAFS	XRD	XAFS	XRD	XAFS	XRD	XAFS	XRD
fresh	0	0	0	0	0.73	0.90	0.27	0.10
reduced at 200 °C	0.70	0.96	0.17	0	0.13	0	0	0.04
reoxidized at 200 °C	0.23	0	0.30	0.31	0.47	0.67	0	0.02
reoxidized at 300 °C	0	0	0		0.70	0.95	0.30	0.05

Figure 7. Cu K-edge XANES data and linear combination fits for the Cu/ceria inverse catalyst, reduced (with CO) and reoxidized (with O$_2$) at 200 °C. The inset shows the raw data obtained at different states of the reaction.

XRD measurement, XAFS results would not indicate their disordered nature; i.e., the XAFS analysis results would have been incomplete or, worse, even misleading. Only when combining the two measurements together in one self-consistent analysis methodology can the new information about the disordered nature of the transient species be obtained. This interpretation agrees well with a similar conclusion made by comparing results of XAFS and neutron diffraction data in experiment with brownmillerite and perovskite materials.[12]

V. SUMMARY AND CONCLUSIONS

In summary, our work demonstrated the uniqueness of the combined use of XAFS and XRD for in situ and operando catalysis studies. Although both of these techniques have been successfully used in catalysis research for many years, too little is known about the advantages and limitations of the simultaneous utilization of these techniques in measuring structure and kinetics in the same catalytic system. In particular, there have been no data available to date that demonstrated the complementary capabilities of the two methods, i.e., when XAFS detects a reaction intermediate while XRD does not, as in the examples shown in our work. However, it is precisely what one expects from the fundamentally different sensitivities of the two techniques, namely, the sensitivity of XRD to the long-range order within the material, and that of XAFS to the nearest environment around absorbing atoms.

In this work we demonstrated how these two methods complement each other in offering better understanding of the structure and kinetics of a catalyst during its chemical treatment. In particular, our studies of inverse Cu/ceria catalyst revealed the formation of strongly disordered, minority species along the two reaction routes: the CO reduction and O$_2$ reoxidation of the catalyst. We showed that independent studies of such systems by either XAFS or XRD alone produce incomplete results.

Our experimental setup offers an exciting new possibility to study heterogeneous catalysis by in situ diffraction anomalous fine structure (DAFS).[29] This method, combining the long-range order sensitivity of XRD and short-range order specificity of XAFS within the same technique, has been used in the past for discriminating between the nanocrystalline and bulk amorphous phases of the same atomic species.[30] In DAFS, a specific phase of

a system is selected by crystallography, as in a conventional XRD experiment, and the local structure of that phase is interrogated by spectroscopy, as in a conventional XAFS experiment. Measurement of the local structure of ordered phases is possible by DAFS because in that experiment Bragg peak intensity is measured as a function of X-ray energy in the resonant scattering region.[29] This hybrid technique allows one in principle to perform in situ, real time chemical speciation and kinetics studies in the system containing reduced and oxidized states of the same catalyst.

Finally, we addressed another important question about the needs to combine these methods in the same experiment, vis-a-vis performing these measurements at two different beamlines, each optimized for in situ, time-resolved XRD, or QEXAFS investigations. We point out that, due to the sample heterogeneities, possible effects of radiation damage, and irreversibility of chemical states before and after the reaction, it is not always possible to repeat the same process at different beamlines. In some cases, however, the reactor cell design and the nature of the process do allow us to reproduce the experiment in virtually identical conditions between the two beamlines, but the combination may still be preferred, if not for any other reason than being a high throughput data collection method. In some cases, however, the all-in-one instrument is less than ideal for high precision structural analyses by, e.g., Rietveld refinement of the XRD data, or multiple-scattering analysis of the EXAFS data, requiring relatively long integration times, and special instruments on dedicated XRD and XAFS beamlines are required. This work shows that the combination of XAFS and XRD in a single experiment is best suited for kinetics studies where the goal is 2-fold: to detect and identify reaction intermediates. Simultaneous XRD and EXAFS experiments capture the same state of the sample from two different perspectives, and thus give a more complete understanding than each of them individually.

■ ASSOCIATED CONTENT

S **Supporting Information.** Mass spectrometry data obtained in the combined XAFS/XRD experiment for reduction and subsequent reoxidation of CeO_2/CuO catalyst. This material is available free of charge via the Internet at http://pubs.acs.org.

■ AUTHOR INFORMATION

Corresponding Author
*E-mail: A.I.F., anatoly.frenkel@yu.edu; J.C.H., hanson1@bnl.gov.

■ ACKNOWLEDGMENT

■ REFERENCES

(1) Phizackerley, R. P.; Rek, Z. U.; Stephenson, G. B.; Conradson, S. D.; Hodgson, K. O.; Matsushita, T.; Oyanagi, H. *J. Appl. Crystallogr.* **1983**, *16*, 220–232.

(2) Tolentino, H.; Baudelet, F.; Dartyge, E.; Fontaine, A.; Lena, A.; Tourillon, G. *Nucl. Instrum. Methods Phys. Res. A* **1990**, *289*, 307–316.

(3) Allen, P. G.; Conradson, S. D.; Penner-Hahn, J. E. *J. Appl. Crystallogr.* **1993**, *26*, 172–179.

(4) Aquilanti, G.; Pascarelli, S. *J. Phys.-Condens. Matter* **2005**, *17*, 1811–1824.

(5) Mathon, O.; Baudelet, F.; Itie, J. P.; Polian, A.; d'Astuto, M.; Chervin, J. C.; Pascarelli, S. *Phys. Rev. Lett.* **2004**, *93*, 255503.

(6) Frahm, R. *Nucl. Instrum. Methods Phys. Res. A* **1988**, *270*, 578–581.

(7) Richwin, M.; Zaeper, R.; Lutzenkirchen-Hecht, D.; Frahm, R. *J. Synchrotron Radiat.* **2001**, *8*, 354–356.

(8) Clausen, B. S.; Grabaek, L.; Steffensen, G.; Hansen, P. L.; Topsoe, H. *Catal. Lett.* **1993**, *20*, 23–36.

(9) Lee, J. M.; Sung, N. E.; Park, J. K.; Yoon, J. G.; Kim, J. H.; Choi, M. H.; Lee, K. B. *J. Synchrotron Radiat.* **1998**, *5*, 524–526.

(10) Norby, P.; Hanson, J. C. *Catal. Today* **1998**, *39*, 301–309.

(11) Wang, X. Q.; Rodriguez, J. A.; Hanson, J. C.; Gamarra, D.; Martinez-Arias, A.; Fernandez-Garcia, M. *J. Phys. Chem. B* **2006**, *110*, 428–434.

(12) Piovano, A.; Agostini, G.; Frenkel, A. I.; Bertier, T.; Prestipino, C.; Ceretti, M.; Paulus, W.; Lamberti, C. *J. Phys. Chem. C* **2011**, *115*, 1311–1322.

(13) Wienold, J; Jentoft, R. E.; Ressler, T. *Eur. J. Inorg. Chem.* **2003**, *6*, 1058–1071.

(14) Grunwaldt, J. D.; Clausen, B. S. *Top. Catal.* **2002**, *18*, 37–43.

(15) Sankar, G.; Thomas, J. M. *Top. Catal.* **1999**, *8*, 1–21.

(16) de Smit, E.; Cinquini, F.; Beale, A. M.; Safonova, O. V.; van Beek, W.; Sautet, P.; Weckhuysen, B. M. *J. Am. Chem. Soc.* **2010**, *132*, 14928–14941.

(17) Ehrlich, S. N.; Hanson, J. C.; Camara, A. L.; Barrio, L.; Estrella, M.; Zhou, G.; Si, R.; Khalid, S.; Wang, Q. *Nucl. Instrum Methods Phys. Res. A* **2011**, *649*, 213–215.

(18) Siddons, D. P.; Hulbert, S. L.; Stephens, P. W. *AIP Conf. Proc.* **2007**, *1767–1770*.

(19) Stern, E. A.; Kim, K. *Phys. Rev. B* **1991**, *23*, 3781–3787.

(20) Estrella, M.; Barrio, L.; Zhou, G.; Wang, X. Q.; Wang, Q.; Wen, W.; Hanson, J. C.; Frenkel, A. I.; Rodriguez, J. A. *J. Phys. Chem. C* **2009**, *113*, 14411–14417.

(21) Krishnan, V.; Selvan, R. K.; Augustin, C. O.; Gedanken, A.; Bertagnolli, H. *J. Phys. Chem. C* **2007**, *111*, 16724–16733.

(22) Toby, B. H. *J. Appl. Crystallogr.* **2005**, *38*, 1040–1041.

(23) Barrio, L.; Estrella, M.; Zhou, G.; Wen, W.; Hanson, J. C.; Hungria, A. B.; Hornes, A.; Fernandez-Garcia, M.; Martinez-Arias, A.; Rodriguez, J. A. *J. Phys. Chem. C* **2010**, *114*, 3580–3587.

(24) Hornes, A.; Hungria, A. B.; Bera, P.; Camara, A. L.; Fernandez-Garcia, M.; Martinez-Arias, A.; Barrio, L.; Estrella, M.; Zhou, G.; Fonseca, J. J.; Hanson, J. C.; Rodriguez, J. A. *J. Am. Chem. Soc.* **2010**, *132*, 34–35.

(25) Hammersley, A. P.; Svensson, S. O.; Thompson, A. *Nucl. Instr. Meth. Phys. Res. A* **1994**, *346*, 312–321.

(26) Rietveld, H. M. *J. Appl. Crystallogr.* **1969**, *2*, 65–71. Toby, B. H. *J. Appl. Crystallogr.* **2001**, *34*, 210–213.

(27) Larson, A. C.; von Dreele, R. B. *GSAS General Structure Analysis System*; Report LAUR 86-748; Los Alamos National Laboratory: Los Alamos, NM, 1995.

(28) This sample was made available courtesy Dr. X. Wang, New Jersey Institute of Technology.

(29) Stragier, H.; Cross, J. O.; Rehr, J. J.; Sorensen, L. B.; Bouldin, C. E.; Woicik, J. C. *Phys. Rev. Lett.* **1992**, *69*, 3064–3067.

(30) Frenkel, A. I.; Kolobov, A. V.; Robinson, I. K.; Cross, J. O.; Maeda, Y.; Bouldin, C. E. *Phys. Rev. Lett.* **2002**, *89*, 285503.

17890

dx.doi.org/10.1021/jp205204e |*J. Phys. Chem. C* 2011, 115, 17884–17890